# Supplemental text, figures, and tables

# "High-resolution reconstructions of South America plate motion relative to Africa, Antarctica, and North America: 34 Ma to present"

*by C. DeMets & S. Merkouriev*

## Overview

The supplementary materials include this document, which has eight figures and five tables that are referenced in the main document, a second document with nine large-scale maps, and a third document with eight tables of rotations in text format, four that reproduce Tables 1 through 4 from the main document and four that reproduce Supplemental Tables 2 through 5 below. All of the supplemental materials are referenced in the main document.

## List of supplementary contents

1. *Supplemental Figures 1 to 8*: These figures show the fits to all 43 fracture zones that were used to estimate the Nubia-South America rotations in this study. Figures 1-3 show the fits in a manner that facilitates more detailed examinations of the fracture zone misfits. Figures 4 to 8 overlay our digitized and predicted fracture zone flow lines on the GeoMapApp bathmetry from which the flow lines were digitized.

2. *Supplemental Table 1*: Summarizes the data inverted to estimate Nubia-South America rotations for all 37 reversals identified in this study and other information pertinent to the reversals and data inversions.

3. *Supplemental Table 2*: Nubia-South America finite rotations that best fit the data listed in Supplemental Table 1. Each rotation is the mean of 1000 rotation sequences that best fit bootstrapped realizations of the data, as described in the main document.

4. *Supplemental Table 3*: This table lists angular velocities that we derived via a REDBACK analysis of the best-fitting Nubia-South America finite rotations in Supplemental Table 2 for a stationary South America plate. The angular velocities are appropriate for calculations of stage velocities in a frame of reference that is tied to the South America plate (such as the stage velocities that are shown in Figure 15a of the main document). The Nubia-South America noise-reduced angular velocities given in Table 2 of the main document are appropriate for velocity calculations in a Nubia plate frame of reference.

5. *Supplemental Table 4*: North America-South America angular velocities determined from the North America-South America finite rotations in Table 3 of the main document and using reversal ages from Supplemental Table 1.

6. *Supplemental Table 5*: Antarctic-South America angular velocities determined from Antarctic-South America finite rotations labeled "noise-reduced" in Table 4 of the main document and using reversal ages from Supplemental Table 1. The footnotes to Table 4 in the main document provide the necessary information about the derivation of the closure-derived Antarctic-South America finite rotations.

7. *Text file with rotations*: This text file contains all of the finite rotations and angular velocities used for the analysis. It is included for reader convenience.

8. *Supplemental Maps 1 to 9*: Due to the large geographic area that is spanned by our study and the abundance of data in many areas, we constructed large-scale maps that subdivide the study area into five regions. Each map displays all the original, along-track magnetic anomaly data within its boundaries overlaid on seafloor bathymetry. The maps also display our magnetic reversal identifications in their original locations as large solid or bold-outlined colored symbols. The small colored symbols filled with aquamarine show each reversal crossing after rotating it from its original location onto the opposite plate with the best-fitting rotations in Supplemental Table 2.

   Each map includes short-hand labels to help identify the ship and airplane tracks. Tracks with labels that begin with "abgt" and "Zarja" are Russian data not previously available for these studies (see Section 2.1 in the main document).

   The small white circles show the digitized fracture zone flow lines described in the main document. Synthetic flow lines constructed with our best-fitting rotations are shown by the small colored circles near the digitized fracture zones. The color-coding scheme used for the synthetic flow lines is the same as for the reversals in the figure.

   For the northernmost region, where the data are relatively sparse, we created only one map (Map 1). For the sub-regions south of the equator, we created two maps per region, one with our identifications of 18 of the 37 reversals and the other with our identifications of the other 19 reversals. Each map includes a legend that identifies the reversals identified on each map and their associated color. None of the maps are captioned.

   Because the native size of all nine maps is 33 by 47 inches, they are well suited for examination at high magnification or printing in large format.

Supplemental Table 1. Data and inversion fitting summary

| Magnetic | Age | Number of data | | | WRMS misfits in km | | |
|---|---|---|---|---|---|---|---|
| reversal | Ma | Anom | FZ | TF | Anom | FZ | TF |
| 1no | 0.781 | 460 | 637 | 2480 | 1.09 | 0.41 | 0.69 |
| 2ny | 1.778 | 458 | 751 | – | 1.74 | 0.74 | – |
| 2An.1y | 2.581 | 475 | 600 | – | 2.01 | 1.12 | – |
| 2An.3o | 3.596 | 438 | 706 | – | 2.32 | 1.36 | – |
| 3n.1y | 4.187 | 363 | 453 | – | 2.28 | 1.46 | – |
| 3n.4o | 5.235 | 342 | 770 | – | 2.19 | 1.61 | – |
| 3An.1y | 6.033 | 286 | 559 | – | 2.27 | 1.96 | – |
| 3An.2o | 6.733 | 268 | 567 | – | 2.52 | 2.04 | – |
| 4n.1y | 7.528 | 260 | 673 | – | 2.32 | 2.04 | – |
| 4n.2o | 8.108 | 233 | 449 | – | 2.76 | 2.03 | – |
| 4Ao | 9.105 | 220 | 797 | – | 2.93 | 2.06 | – |
| 5n.1y | 9.786 | 224 | 544 | – | 2.85 | 2.04 | – |
| 5n.2o | 11.056 | 219 | 1074 | – | 2.72 | 2.27 | – |
| 5An.2o | 12.474 | 197 | 1303 | – | 2.60 | 2.60 | – |
| 5ACy | 13.739 | 195 | 1238 | – | 2.95 | 3.06 | – |
| 5ADo | 14.609 | 208 | 844 | – | 2.72 | 3.15 | – |
| 5Cn.1y | 15.974 | 186 | 1150 | – | 2.79 | 3.62 | – |
| 5Dy | 17.235 | 149 | 1027 | – | 2.89 | 3.46 | – |
| 5Ey | 18.056 | 153 | 747 | – | 2.84 | 3.24 | – |
| 6ny | 18.748 | 117 | 683 | – | 3.74 | 3.28 | – |
| 6no | 19.722 | 124 | 860 | – | 3.09 | 3.47 | – |
| 6An.2o | 20.709 | 92 | 955 | – | 3.09 | 3.31 | – |
| 6Bn.1y | 21.767 | 85 | 957 | – | 3.88 | 3.51 | – |
| 7n.1y | 23.962 | 78 | 1784 | – | 3.38 | 3.93 | – |
| 7n.2o | 24.474 | 76 | 283 | – | 3.47 | 4.42 | – |
| 8n.1y | 25.099 | 87 | 590 | – | 3.72 | 4.18 | – |
| 8n.2o | 25.987 | 79 | 500 | – | 3.56 | 4.20 | – |
| 9ny | 26.420 | 83 | 478 | – | 3.97 | 4.53 | – |
| 9no | 27.439 | 76 | 554 | – | 3.38 | 4.34 | – |
| 10n.1y | 27.859 | 82 | 338 | – | 2.34 | 5.15 | – |
| 10n.2o | 28.278 | 79 | 291 | – | 3.09 | 5.40 | – |
| 11n.1y | 29.183 | 88 | 585 | – | 4.20 | 5.69 | – |
| 11n.2o | 29.970 | 85 | 430 | – | 4.07 | 5.49 | – |
| 12ny | 30.591 | 80 | 351 | – | 2.69 | 5.52 | – |
| 12no | 31.034 | 85 | 269 | – | 3.74 | 5.07 | – |
| 13ny | 33.157 | 110 | 1373 | – | 2.98 | 4.87 | – |
| 13no | 33.705 | 112 | 240 | – | 3.38 | 5.19 | – |

The letters ”o” and ”y” that are appended to the magnetic reversal identifiers respectively indicate the old or young edge of the magnetic reversal. Reversal ages are from the GTS12 time scale (Hilgen et al. 2012; Ogg 2012). Anom, FZ, and TF respectively indicate the number of magnetic reversal, fracture zone, and transform fault crossings used to estimate the finite rotations listed in

subsequent. Ages estimated for the fracture zone crossings are approximated from their distances along their respective flow lines, although in the inversion, every fracture zone crossing contributes information to the finite rotation estimates for each chron. WRMS is the weighted root-mean-square misfit in km of the best-fitting rotation adjusted for the number of parameters that were estimated in order to fit the given data subset.

Supplemental Table 2. Nubia-South America best-fitting finite rotations

| Chron | DOF | Lat. | Long. | Ω | Covariances from bootstrap procedure | | | | | |
|---|---|---|---|---|---|---|---|---|---|---|
| | | (°N) | (°E) | (degrees) | a | b | c | d | e | f |
| 1n | 3574 | 60.09 | 321.45 | -0.219 | 4.9 | -1.4 | 1.1 | 4.0 | 0.1 | 6.9 |
| 2n | 1206 | 61.11 | 321.44 | -0.513 | 66.9 | 11.8 | -1.2 | 49.2 | 3.6 | 34.1 |
| 2An.1 | 1072 | 62.55 | 317.74 | -0.757 | 887.3 | 202.4 | -238.9 | 100.0 | -47.8 | 108.8 |
| 2An.3 | 1141 | 63.13 | 320.23 | -1.038 | 161.6 | 24.1 | -50.9 | 87.0 | 19.8 | 73.5 |
| 3n.1 | 813 | 62.62 | 319.37 | -1.223 | 167.3 | 8.8 | -40.3 | 65.1 | 4.9 | 45.0 |
| 3n.4 | 996 | 61.22 | 320.28 | -1.549 | 168.8 | 40.1 | -23.9 | 105.9 | -5.5 | 41.8 |
| 3An.1 | 774 | 61.89 | 320.53 | -1.776 | 260.1 | 26.2 | -46.2 | 239.2 | 38.1 | 74.4 |
| 3An.2 | 752 | 61.51 | 319.62 | -2.007 | 301.4 | 65.1 | -46.4 | 104.3 | -3.6 | 77.7 |
| 4n.1 | 854 | 59.99 | 321.10 | -2.303 | 210.1 | 57.3 | -16.0 | 76.4 | 4.1 | 48.4 |
| 4n.2 | 619 | 61.29 | 320.11 | -2.498 | 447.5 | 35.2 | -47.2 | 108.3 | -15.5 | 114.7 |
| 4A | 950 | 61.33 | 320.03 | -2.868 | 425.9 | 26.4 | -34.0 | 105.4 | -16.7 | 202.2 |
| 5n.1 | 705 | 61.32 | 319.72 | -3.120 | 342.8 | 43.2 | -47.5 | 98.3 | -2.5 | 106.3 |
| 5n.2 | 1234 | 61.08 | 320.54 | -3.617 | 774.4 | 135.2 | -95.1 | 148.8 | 5.8 | 132.3 |
| 5An.2 | 1447 | 61.80 | 319.55 | -4.193 | 1039.5 | 152.5 | -178.9 | 166.1 | 18.4 | 122.1 |
| 5AC | 1394 | 61.82 | 319.73 | -4.750 | 881.0 | -18.4 | -33.7 | 310.0 | 28.5 | 99.1 |
| 5AD | 1011 | 59.84 | 321.39 | -5.163 | 505.5 | 72.9 | -10.2 | 393.0 | 51.2 | 54.4 |
| 5Cn.1 | 1291 | 60.95 | 320.71 | -5.729 | 508.9 | 120.5 | -31.3 | 324.7 | -1.4 | 91.0 |
| 5D | 1127 | 59.98 | 321.61 | -6.278 | 344.2 | 36.0 | -48.9 | 215.3 | 3.7 | 175.4 |
| 5E | 853 | 60.24 | 321.67 | -6.661 | 517.7 | -66.6 | -15.0 | 195.0 | -22.1 | 170.4 |
| 6ny | 753 | 60.49 | 321.59 | -7.023 | 660.8 | -69.5 | -81.8 | 194.5 | -42.2 | 285.7 |
| 6no | 929 | 60.61 | 321.57 | -7.467 | 530.1 | 15.7 | -76.1 | 171.8 | -15.8 | 113.9 |
| 6An.2 | 1047 | 60.41 | 321.76 | -7.972 | 670.0 | -32.5 | -83.9 | 222.6 | -16.3 | 233.7 |
| 6Bn.1 | 1042 | 60.01 | 322.34 | -8.479 | 1354.1 | 378.0 | -287.2 | 734.3 | -43.4 | 448.9 |
| 7n.1 | 1862 | 58.52 | 323.54 | -9.464 | 1045.9 | 411.7 | -200.3 | 971.7 | 85.8 | 427.4 |
| 7n.2 | 359 | 58.92 | 323.21 | -9.620 | 653.0 | 293.0 | -50.9 | 768.5 | 32.8 | 291.9 |
| 8n.1 | 677 | 58.44 | 323.63 | -9.962 | 960.7 | 43.8 | 11.6 | 836.4 | -50.4 | 525.7 |
| 8n.2 | 579 | 57.91 | 324.07 | -10.252 | 685.1 | -11.3 | 142.7 | 448.6 | -62.0 | 320.2 |
| 9ny | 561 | 58.20 | 324.01 | -10.534 | 861.3 | -21.1 | 11.9 | 597.0 | -46.9 | 330.9 |
| 9no | 630 | 57.24 | 324.68 | -10.868 | 496.1 | 86.8 | -40.3 | 432.1 | -6.7 | 321.0 |
| 10n.1 | 420 | 57.32 | 324.58 | -11.082 | 537.2 | -113.0 | 20.4 | 321.0 | -20.2 | 124.6 |
| 10n.2 | 370 | 57.17 | 324.83 | -11.277 | 1018.7 | -137.5 | -37.8 | 383.3 | -43.5 | 323.9 |
| 11n.1 | 673 | 57.55 | 324.84 | -11.639 | 1395.7 | -135.5 | -25.5 | 757.7 | -74.1 | 413.7 |
| 11n.2 | 515 | 57.07 | 325.18 | -11.939 | 1094.5 | -216.2 | 155.8 | 552.3 | -58.1 | 362.5 |
| 12ny | 431 | 57.23 | 325.15 | -12.161 | 545.6 | -84.4 | 29.9 | 406.6 | -13.9 | 175.2 |
| 12no | 354 | 57.07 | 325.35 | -12.353 | 664.7 | -128.3 | 59.5 | 467.1 | -32.5 | 243.4 |
| 13ny | 1483 | 56.85 | 325.78 | -13.373 | 673.5 | 15.8 | -26.5 | 808.3 | 80.2 | 150.2 |
| 13no | 352 | 56.78 | 325.69 | -13.580 | 1261.4 | 77.9 | -177.4 | 583.7 | -32.0 | 259.5 |

These finite rotations reconstruct movement of the Nubia plate relative to the South America plate and include a 2-km correction for outward displacement. The rotation angles Ω are positive CCW. Each rotation is the mean of 1000 bootstrap solutions (see text). DOF, the degrees of freedom, equals the total number of magnetic reversal, transform fault, and fracture zone flow-line crossings

used to estimate the rotation for a given time reduced by the number of estimated parameters. The weighted RMS misfits for these rotations are given in Supplemental Table 1. The bootstrap-derived Cartesian rotation covariances, which specify the 2-D position uncertainty when rotating points from the Nubia onto the South America plate or vice versa, and have units of $10^{-10}$ radians$^2$. See footnotes to Table 1 in the main document for information on how to build the rotation covariance matrix from the elements in the table.

Supplemental Table 3. Nubia-South America stage angular velocities from REDBACK

| Age(y) | Age(o) | Lat. | Long. | $\dot{\omega}$ | Covariances | | | | | |
|---|---|---|---|---|---|---|---|---|---|---|
| (Ma) | (Ma) | (°N) | (°E) | ° Myr$^{-1}$ | a | b | c | d | e | f |
| 0.000 | 0.781 | 60.35 | 321.26 | 0.284 | 7.23 | -5.78 | 16.04 | 4.64 | -12.87 | 36.29 |
| 0.781 | 1.778 | 60.79 | 320.79 | 0.287 | 1.61 | -1.16 | 2.86 | 0.96 | -2.35 | 6.92 |
| 1.778 | 2.581 | 61.15 | 320.37 | 0.292 | 1.37 | -0.79 | 1.54 | 0.71 | -1.37 | 4.37 |
| 2.581 | 3.596 | 61.35 | 320.11 | 0.300 | 1.27 | -0.68 | 1.19 | 0.62 | -1.10 | 3.67 |
| 3.596 | 4.187 | 61.41 | 320.02 | 0.306 | 1.39 | -0.77 | 1.38 | 0.74 | -1.26 | 4.20 |
| 4.187 | 5.235 | 61.42 | 319.99 | 0.309 | 1.35 | -0.78 | 1.53 | 0.71 | -1.38 | 4.42 |
| 5.235 | 6.033 | 61.43 | 319.97 | 0.311 | 1.73 | -1.00 | 2.02 | 0.89 | -1.84 | 5.80 |
| 6.033 | 6.733 | 61.40 | 320.01 | 0.331 | 2.33 | -1.38 | 2.86 | 1.21 | -2.59 | 8.14 |
| 6.733 | 7.528 | 61.36 | 320.07 | 0.355 | 2.52 | -1.33 | 2.27 | 1.16 | -2.18 | 7.24 |
| 7.528 | 8.108 | 61.35 | 320.11 | 0.359 | 2.79 | -1.33 | 1.99 | 1.17 | -2.04 | 7.00 |
| 8.108 | 9.105 | 61.28 | 320.24 | 0.361 | 2.92 | -1.26 | 1.64 | 1.09 | -1.83 | 6.48 |
| 9.105 | 9.786 | 61.13 | 320.46 | 0.367 | 4.08 | -1.90 | 2.93 | 1.65 | -3.07 | 10.37 |
| 9.786 | 11.056 | 60.88 | 320.81 | 0.387 | 4.88 | -2.42 | 4.30 | 2.07 | -4.28 | 13.87 |
| 11.056 | 12.474 | 60.36 | 321.45 | 0.423 | 3.96 | -1.74 | 2.35 | 1.54 | -2.57 | 9.07 |
| 12.474 | 13.739 | 59.62 | 322.28 | 0.436 | 3.53 | -1.54 | 0.97 | 1.41 | -1.34 | 6.21 |
| 13.739 | 14.609 | 59.04 | 322.89 | 0.438 | 9.02 | -3.18 | -2.03 | 2.27 | -0.29 | 7.84 |
| 14.609 | 15.974 | 58.94 | 323.17 | 0.438 | 4.01 | -1.86 | 0.52 | 1.54 | -1.02 | 6.19 |
| 15.974 | 17.235 | 58.53 | 323.64 | 0.446 | 4.36 | -2.00 | 0.76 | 1.63 | -1.25 | 6.81 |
| 17.235 | 18.056 | 58.29 | 323.93 | 0.463 | 6.27 | -3.00 | 1.78 | 2.40 | -2.29 | 11.05 |
| 18.056 | 18.748 | 58.07 | 324.18 | 0.474 | 7.93 | -3.71 | 1.34 | 2.97 | -2.27 | 12.77 |
| 18.748 | 19.722 | 57.59 | 324.59 | 0.479 | 9.09 | -4.17 | 1.28 | 3.41 | -2.34 | 13.85 |
| 19.722 | 20.709 | 56.56 | 325.28 | 0.481 | 10.89 | -5.03 | 1.95 | 4.20 | -2.98 | 16.89 |
| 20.709 | 21.767 | 54.86 | 326.26 | 0.477 | 12.35 | -5.54 | -0.46 | 4.57 | -1.36 | 15.05 |
| 21.767 | 23.962 | 51.82 | 327.91 | 0.446 | 10.66 | -4.73 | -3.11 | 3.49 | 0.72 | 9.34 |
| 23.962 | 24.474 | 50.09 | 328.94 | 0.430 | 20.23 | -8.32 | -8.81 | 5.72 | 3.13 | 13.28 |
| 24.474 | 25.099 | 49.71 | 329.23 | 0.429 | 19.95 | -7.82 | -9.98 | 5.22 | 3.77 | 11.50 |
| 25.099 | 25.987 | 49.42 | 329.58 | 0.427 | 16.89 | -6.27 | -9.15 | 4.36 | 3.54 | 9.14 |
| 25.987 | 26.420 | 49.41 | 329.80 | 0.426 | 19.31 | -6.84 | -10.91 | 5.02 | 4.26 | 10.08 |
| 26.420 | 27.439 | 50.08 | 329.84 | 0.425 | 14.86 | -4.98 | -8.29 | 3.87 | 3.08 | 7.95 |
| 27.439 | 27.859 | 51.46 | 329.64 | 0.423 | 18.44 | -5.82 | -10.39 | 4.73 | 3.80 | 9.40 |
| 27.859 | 28.278 | 52.23 | 329.50 | 0.422 | 17.11 | -5.29 | -9.46 | 4.34 | 3.36 | 8.79 |
| 28.278 | 29.183 | 53.46 | 329.23 | 0.421 | 10.66 | -3.43 | -5.37 | 2.91 | 1.84 | 6.13 |
| 29.183 | 29.970 | 54.38 | 329.05 | 0.421 | 8.75 | -3.10 | -3.63 | 2.91 | 1.23 | 6.25 |
| 29.970 | 30.591 | 54.70 | 329.03 | 0.421 | 8.37 | -3.11 | -3.16 | 3.11 | 1.14 | 6.45 |
| 30.591 | 31.034 | 54.81 | 329.07 | 0.423 | 8.60 | -3.29 | -3.00 | 3.39 | 1.08 | 6.98 |
| 31.034 | 33.157 | 54.81 | 329.28 | 0.428 | 9.43 | -3.67 | -3.34 | 3.98 | 1.30 | 7.82 |
| 33.157 | 33.705 | 54.58 | 329.65 | 0.429 | 21.19 | -7.30 | -3.71 | 9.08 | 0.17 | 20.96 |

These angular velocities specify Nubia plate motion in a South America plate frame of reference for time intervals given in the first two columns, as determined from the REDBACK noise-reduction software (Iaffaldano *et al*. 2014). They include corrections for 2 km of outward displacement, as described in the text. The angular rotation rates $\dot{\omega}$ are positive anti-clockwise. The Cartesian angular velocity covariances are calculated in a frame of reference tied to the South America plate and have units of $10^{-8}$ radians$^2$ Myr$^{-2}$.

Supplemental Table 4. North America-South America stage angular velocities

| Age(y) | Age(o) | Lat. | Long. | $\dot{\Omega}$ | Covariances | | | | | |
|---|---|---|---|---|---|---|---|---|---|---|
| Ma | Ma | (°N) | (°E) | ° $Myr^{-1}$ | a | b | c | d | e | f |
| 0.781 | 0.00 | 9.53 | -56.96 | 0.133 | 1.33 | -0.16 | 0.25 | 0.66 | -0.83 | 1.04 |
| 1.778 | 0.781 | 11.32 | -57.30 | 0.138 | 1.69 | -0.13 | 0.19 | 0.86 | -1.08 | 1.38 |
| 2.581 | 1.778 | 13.04 | -57.32 | 0.144 | 2.92 | -0.01 | -0.05 | 1.50 | -1.93 | 2.57 |
| 3.596 | 2.581 | 15.36 | -56.62 | 0.153 | 2.17 | 0.16 | -0.38 | 1.10 | -1.46 | 2.08 |
| 4.187 | 3.596 | 16.68 | -55.95 | 0.159 | 7.42 | 1.06 | -2.32 | 3.69 | -5.06 | 7.61 |
| 5.235 | 4.187 | 17.02 | -55.36 | 0.162 | 2.73 | 0.59 | -1.23 | 1.36 | -1.92 | 3.05 |
| 6.033 | 5.235 | 17.02 | -54.78 | 0.165 | 5.69 | 1.37 | -3.00 | 2.88 | -4.22 | 6.96 |
| 6.733 | 6.033 | 19.52 | -53.87 | 0.180 | 8.72 | 1.94 | -4.59 | 4.39 | -6.57 | 11.24 |
| 7.528 | 6.733 | 18.10 | -53.91 | 0.194 | 7.83 | 1.49 | -3.81 | 3.55 | -5.44 | 9.97 |
| 8.108 | 7.528 | 15.67 | -54.27 | 0.195 | 17.77 | 2.40 | -6.58 | 6.76 | -10.43 | 21.05 |
| 9.105 | 8.108 | 15.41 | -54.04 | 0.199 | 8.37 | 0.57 | -1.68 | 2.67 | -4.00 | 8.98 |
| 9.786 | 9.105 | 16.11 | -53.78 | 0.205 | 25.44 | 0.94 | -2.21 | 7.32 | -10.43 | 25.70 |
| 11.056 | 9.786 | 19.62 | -53.06 | 0.216 | 10.60 | 0.35 | -0.46 | 2.89 | -4.04 | 10.64 |
| 12.474 | 11.056 | 24.97 | -53.05 | 0.239 | 12.01 | 0.58 | -0.80 | 3.09 | -4.53 | 12.38 |
| 13.739 | 12.474 | 22.52 | -55.55 | 0.229 | 19.24 | 1.48 | -1.47 | 4.46 | -6.81 | 19.32 |
| 14.609 | 13.739 | 13.52 | -59.82 | 0.205 | 48.58 | 3.75 | -0.09 | 9.46 | -14.27 | 43.31 |
| 15.974 | 14.609 | 13.29 | -62.30 | 0.182 | 21.90 | 0.34 | 2.14 | 3.50 | -5.54 | 17.07 |
| 17.235 | 15.974 | 15.48 | -61.58 | 0.173 | 25.85 | -1.82 | 3.81 | 3.85 | -6.74 | 19.01 |
| 18.056 | 17.235 | 20.06 | -59.66 | 0.174 | 59.35 | -7.51 | 8.83 | 9.30 | -16.80 | 43.89 |
| 18.748 | 18.056 | 23.32 | -57.76 | 0.175 | 87.51 | -13.73 | 14.21 | 14.30 | -25.94 | 65.42 |
| 19.722 | 18.748 | 27.88 | -57.50 | 0.150 | 50.24 | -11.24 | 10.91 | 10.79 | -18.30 | 40.60 |

Angular velocities that specify the movement of the North America plate relative to South America for the time period given in the first two columns. The angular velocities and their Cartesian covariances are derived from the finite rotations given in Table 3 of the main document and are in a South America plate reference frame. The angular rotation rates $\dot{\omega}$ are positive anticlockwise for the old to the young limit of each time interval. The covariances have units of $10^{-8}$ radians$^2$ $Myr^{-2}$. See Table 1 in the main document for instructions on constructing the covariance matrix from elements a-f in the table.

Supplemental Table 5. Antarctica-South America angular velocities

| Age(y) | Age(o) | Lat. | Long. | $\dot{\Omega}$ | Covariances | | | | | |
|---|---|---|---|---|---|---|---|---|---|---|
| Ma | Ma | (°N) | (°E) | ° $Myr^{-1}$ | a | b | c | d | e | f |
| 0.781 | 0.00 | -85.92 | 36.10 | 0.263 | 1.87 | -1.28 | 0.48 | 0.96 | -0.45 | 1.53 |
| 1.778 | 0.781 | -85.89 | 44.37 | 0.271 | 2.50 | -1.57 | 0.54 | 1.23 | -0.47 | 2.02 |
| 2.581 | 1.778 | -85.72 | 49.02 | 0.280 | 4.69 | -2.41 | 0.71 | 2.12 | -0.50 | 3.71 |
| 3.596 | 2.581 | -85.74 | 56.89 | 0.288 | 3.82 | -1.47 | 0.32 | 1.53 | -0.12 | 2.96 |
| 4.187 | 3.596 | -85.93 | 65.58 | 0.290 | 13.91 | -4.14 | 0.32 | 5.09 | 0.46 | 10.57 |
| 5.235 | 4.187 | -85.84 | 89.96 | 0.285 | 5.17 | -1.26 | -0.25 | 1.74 | 0.36 | 3.85 |
| 6.033 | 5.235 | -84.75 | 110.33 | 0.280 | 11.00 | -2.61 | -1.28 | 3.59 | 0.88 | 8.10 |
| 6.733 | 6.033 | -84.15 | 110.42 | 0.299 | 18.17 | -4.53 | -3.00 | 5.88 | 1.72 | 13.21 |
| 7.528 | 6.733 | -84.25 | 103.56 | 0.324 | 16.87 | -3.74 | -3.32 | 5.19 | 1.75 | 12.17 |
| 8.108 | 7.528 | -84.61 | 96.12 | 0.328 | 35.93 | -6.63 | -7.13 | 10.50 | 2.99 | 26.13 |
| 9.105 | 8.108 | -84.82 | 90.68 | 0.329 | 14.59 | -2.28 | -2.41 | 4.11 | 0.33 | 10.90 |
| 9.786 | 9.105 | -84.70 | 94.02 | 0.330 | 38.17 | -5.32 | -5.23 | 10.50 | -1.36 | 29.24 |
| 11.056 | 9.786 | -83.61 | 105.98 | 0.349 | 13.77 | -1.70 | -1.87 | 3.62 | -1.23 | 10.74 |
| 12.474 | 11.056 | -81.66 | 116.78 | 0.388 | 13.91 | -1.16 | -2.38 | 3.30 | -1.58 | 10.90 |
| 13.739 | 12.474 | -81.14 | 120.70 | 0.403 | 19.64 | -0.33 | -4.15 | 4.04 | -1.80 | 15.31 |
| 14.609 | 13.739 | -80.78 | 124.47 | 0.404 | 43.62 | 1.86 | -8.96 | 8.32 | -2.06 | 34.06 |
| 15.974 | 14.609 | -81.03 | 128.18 | 0.403 | 20.45 | 1.44 | -2.55 | 4.15 | 0.44 | 16.08 |
| 17.235 | 15.974 | -79.36 | 139.82 | 0.397 | 30.62 | 3.09 | 0.34 | 6.73 | 2.99 | 24.36 |
| 18.056 | 17.235 | -77.46 | 146.75 | 0.394 | 87.49 | 12.59 | 10.29 | 19.90 | 13.24 | 70.97 |
| 18.748 | 18.056 | -73.28 | 162.66 | 0.346 | 137.15 | 25.30 | 23.94 | 30.91 | 24.78 | 113.22 |
| 19.722 | 18.748 | -53.95 | 196.18 | 0.347 | 70.41 | 13.06 | 10.27 | 14.77 | 11.40 | 58.20 |

Angular velocities that specify Antarctic plate motion relative to South America during the time period given in the first two columns. The angular velocities and their Cartesian covariances are in a South America plate reference frame and are derived from the noise-reduced finite rotations in Table 4 of the main document. The angular rotation rates $\dot{\omega}$ are positive anticlockwise for the old to the young limit of each time interval. The covariances have units of $10^{-7}$ radians$^2$ $Myr^{-2}$. See Table 1 footnotes from the main document for instructions on constructing the covariance matrix from elements a-f in the table.

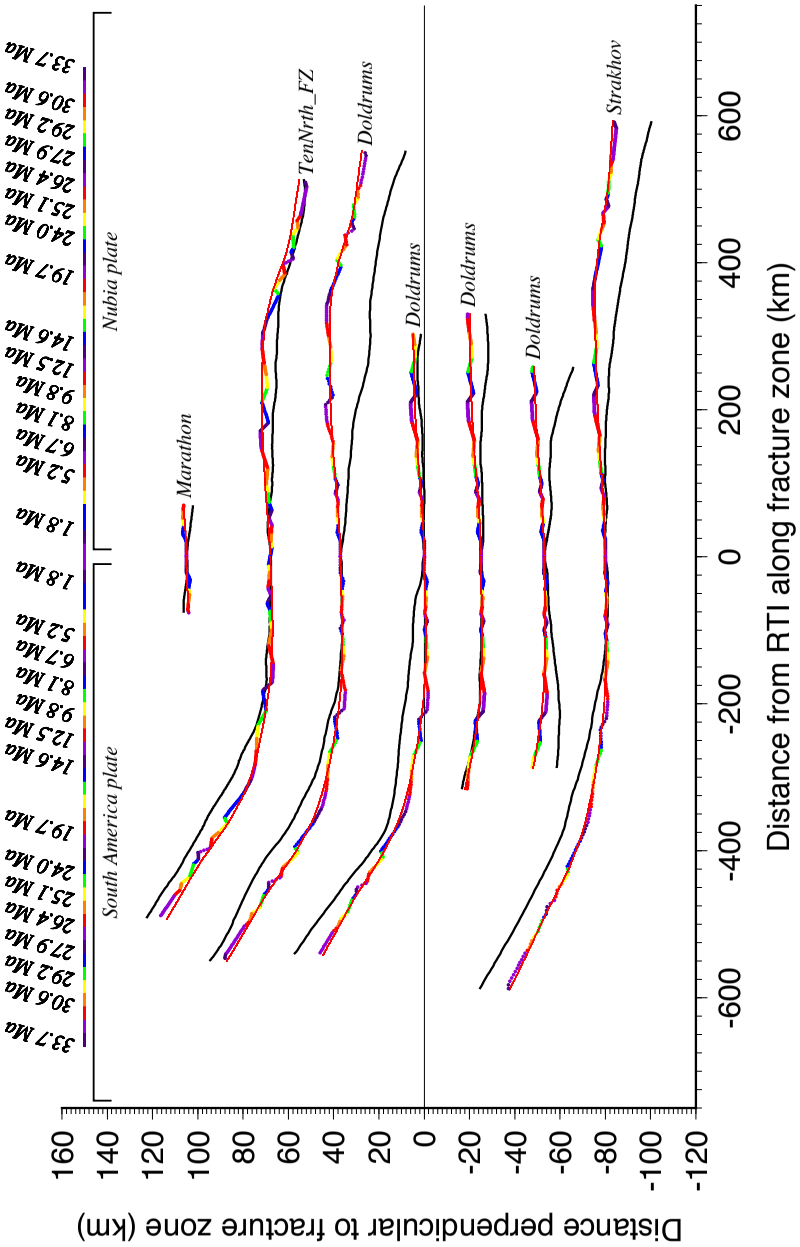


Supplemental Figure 1. Digitized fracture zone traces (black) compared to best-fitting (color-coded lines) and noise-reduced (red lines) synthetic fracture zone traces, 2-15°N. The flow lines, which are created with the rotations in Supplemental Table 2 and Table 1 of the main document, assume symmetric seafloor spreading. The same fracture zones and flow lines are shown with bathymetry in Figure 5 of the main document and Supplemental Figure 8a. Horizontal and vertical axes respectively show linear distance along or orthogonal to each fracture zone. Vertical-axis distances are exaggerated by three times relative to horizontal distances to emphasize the misfits. Zero distance on the horizontal axis marks the ridge-transform intersection for fracture zones that extend to the ridge or the youngest off-axis fracture zone point. Transform faults are omitted from this plot.

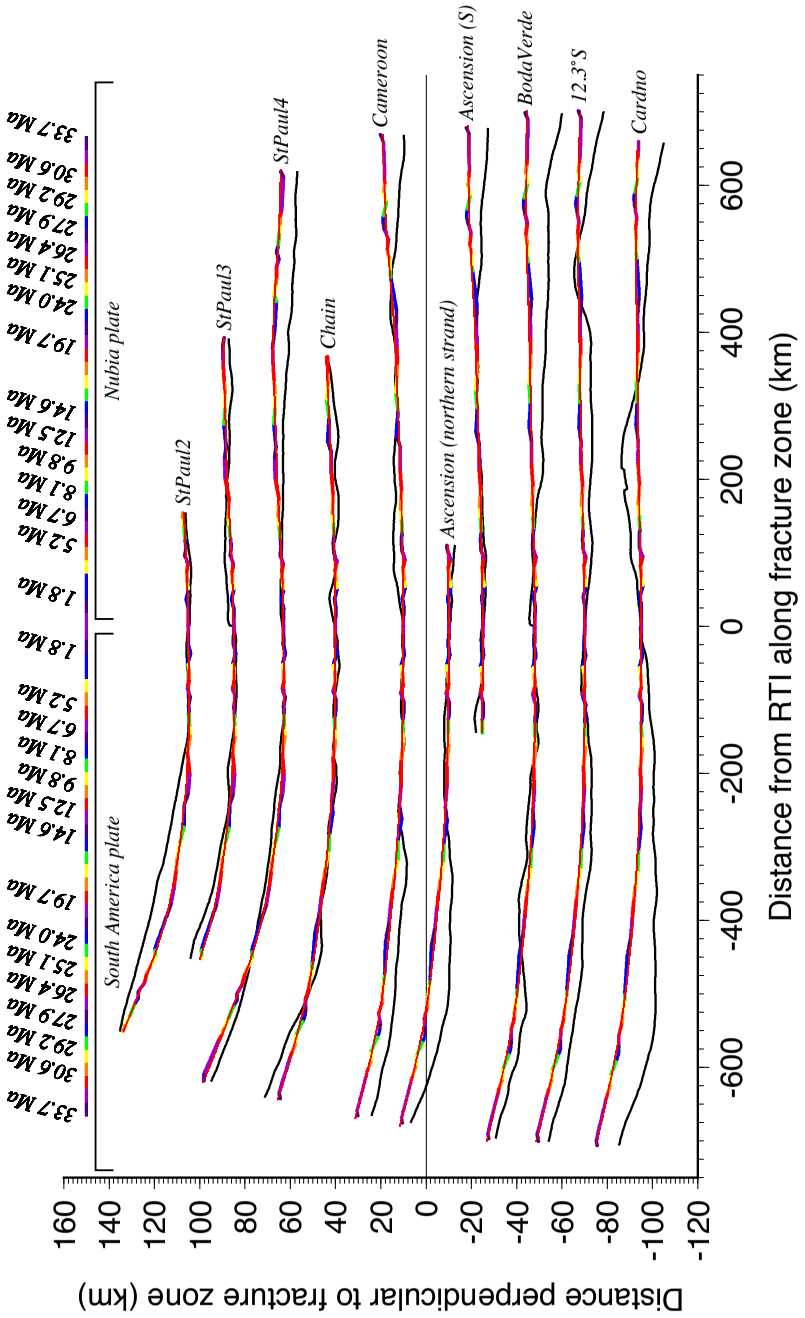


Supplemental Figure 2. Digitized fracture zone traces (black) compared to best-fitting (color-coded lines) and noise-reduced (red lines) synthetic fracture zone traces, 2°N-15°S. The same fracture zones and flow lines are shown with bathymetry in Supplemental Figures 4 and 5. See the caption to Supplemental Figure 1 for further information.

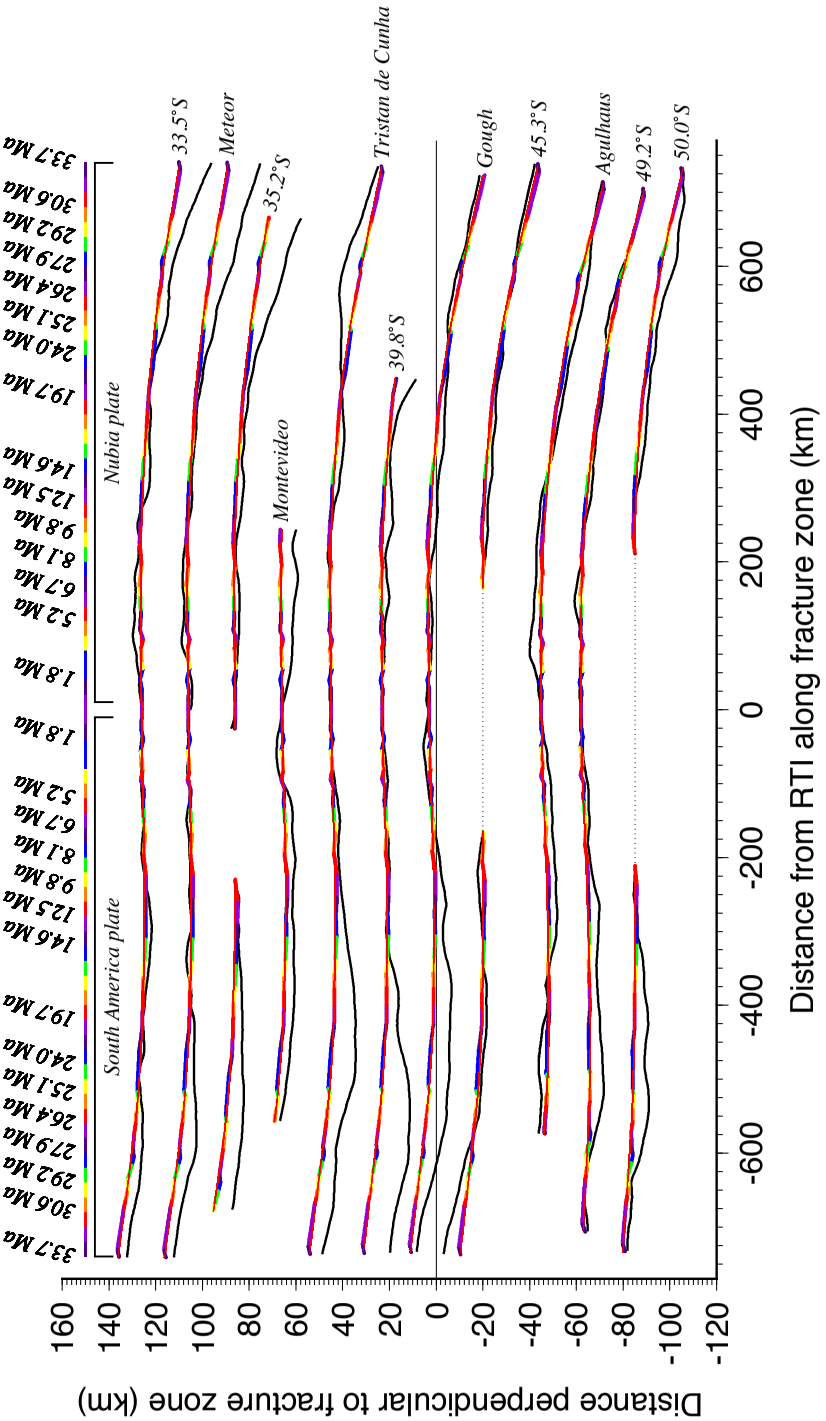


Supplemental Figure 3. Digitized fracture zone traces (black) compared to best-fitting (color-coded lines) and noise-reduced (red lines) synthetic fracture zone traces, 33-50°S. The same fracture zones and flow lines are shown with bathymetry in Supplemental Figures 7 and 8. See the caption to Supplemental Figure 1 for further information.

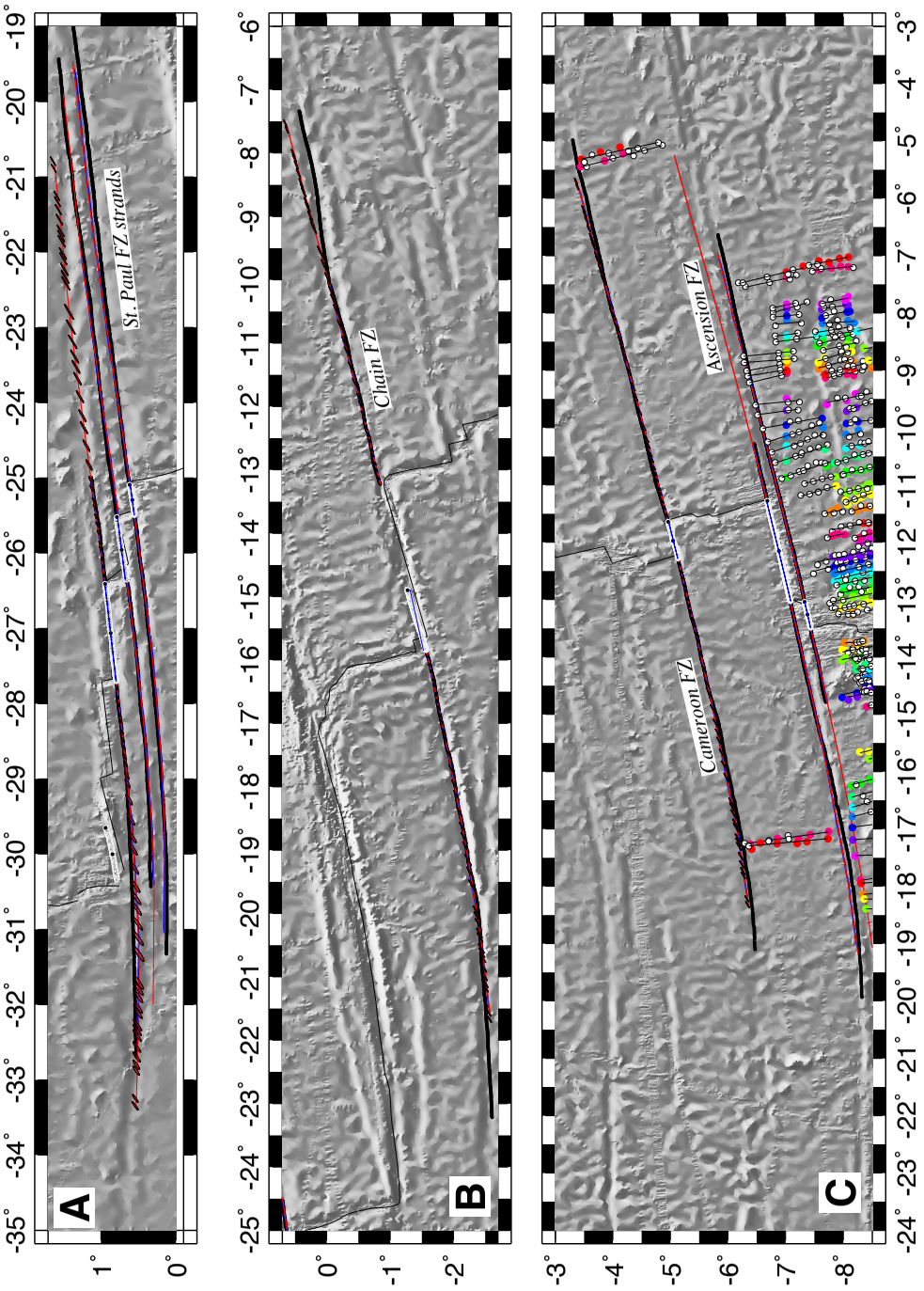


Supplemental Figure 4. Reconstructed (blue and red) and digitized (black) Nubia-South America fracture zone flow lines and transform faults and fracture zone crossings overlaid on GeoMapApp bathymetry, 2°N-8°S. Blue and red lines are best-fitting and noise-reduced flow lines, respectively. Solid circles are reversal identifications at their original locations. Open circles are reversal crossings rotated onto the opposite side of the ridge with the best-fitting rotations in Supplemental Table 2. The red-shaded ellipses for selected flow lines show the 1-$\sigma$ uncertainties propagated from the noise-reduced rotation covariances. Reconstructions and the original magnetic data for the entire study area are shown at larger scale in Supplemental Maps 1 to 9.

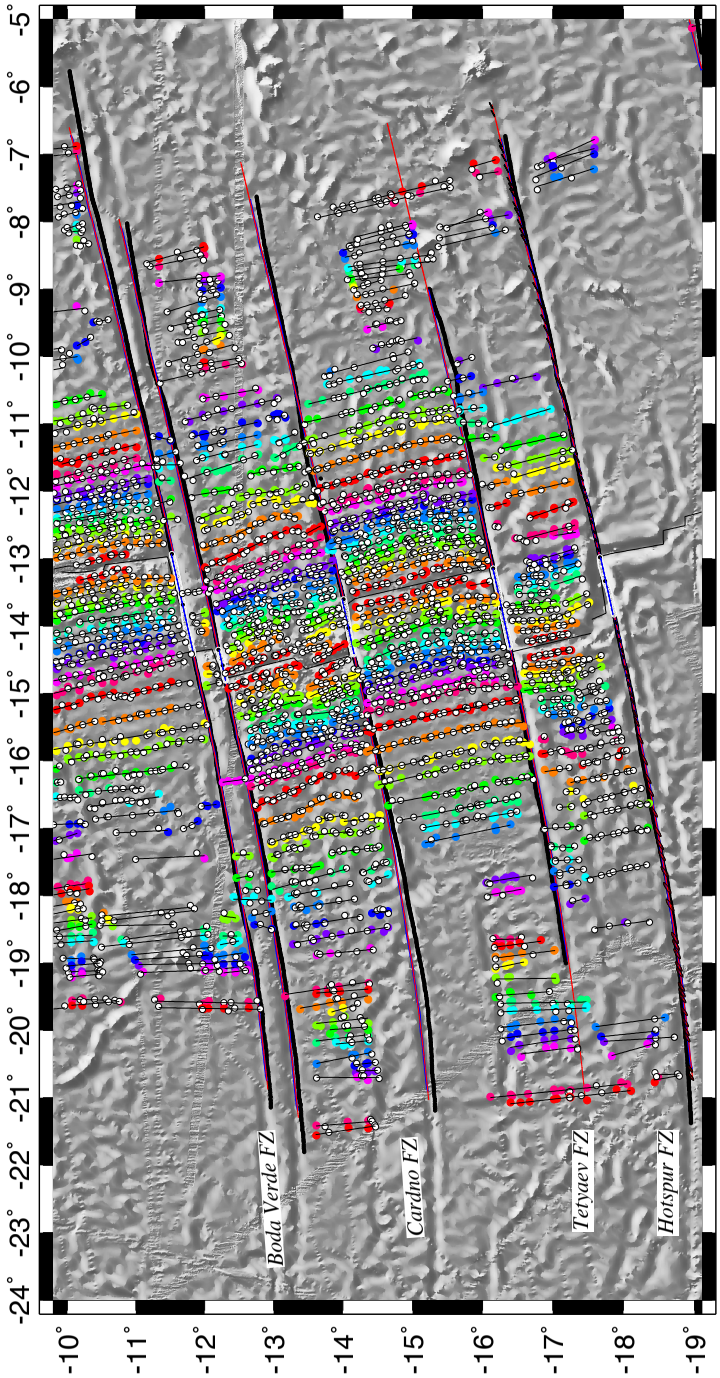


Supplemental Figure 5. Reconstructed (blue and red) and digitized (black) Nubia-South America fracture zone flow lines and transform faults and fracture zone crossings overlaid on GeoMapApp bathymetry, 10°S-19°S. See the caption to Supplemental Figure 4 for further information.

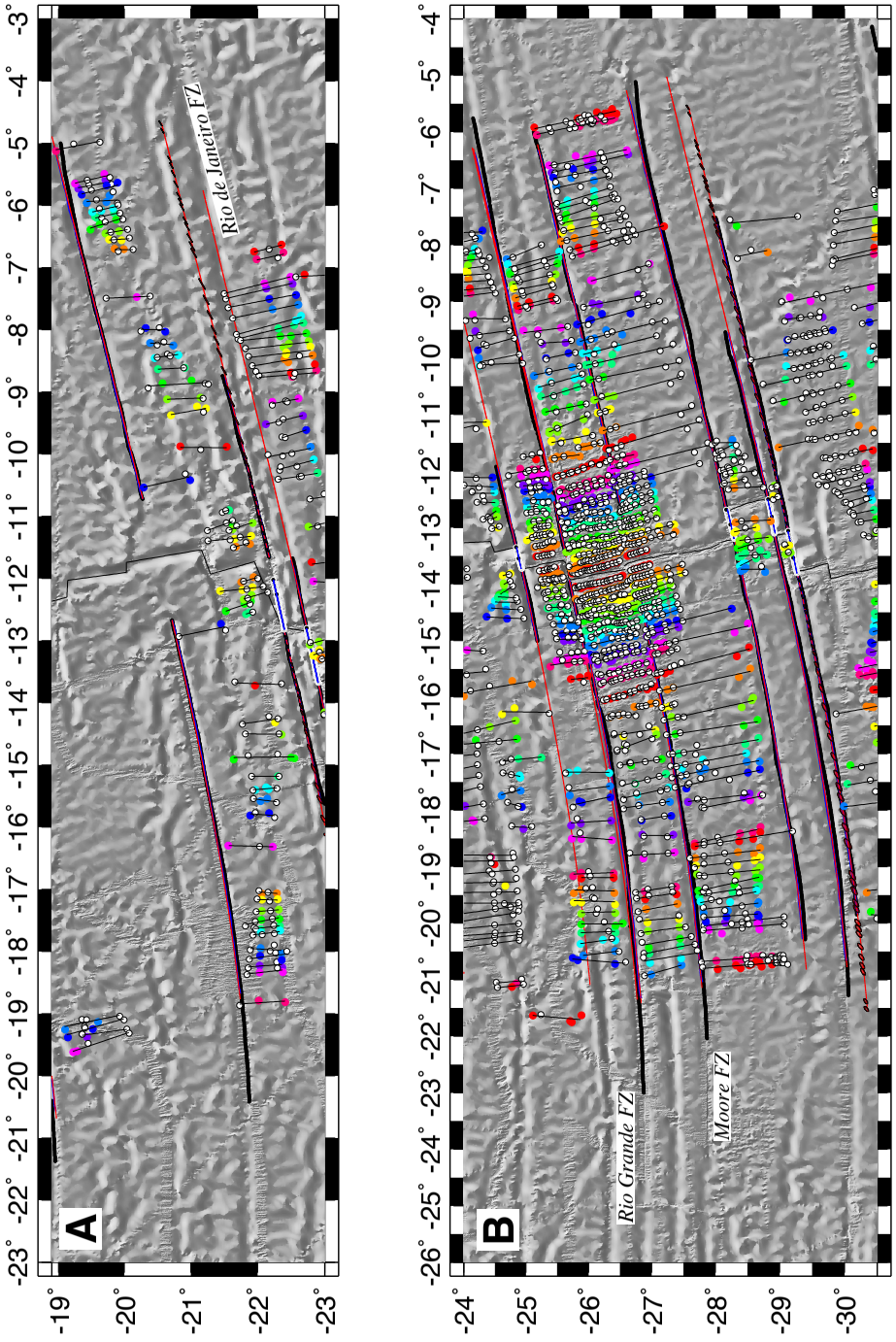


Supplemental Figure 6. Reconstructed (blue and red) and digitized (black) Nubia-South America fracture zone flow lines and transform faults and fracture zone crossings overlaid on GeoMapApp bathymetry, 19°S-30°S. See the caption to Supplemental Figure 4 for further information.

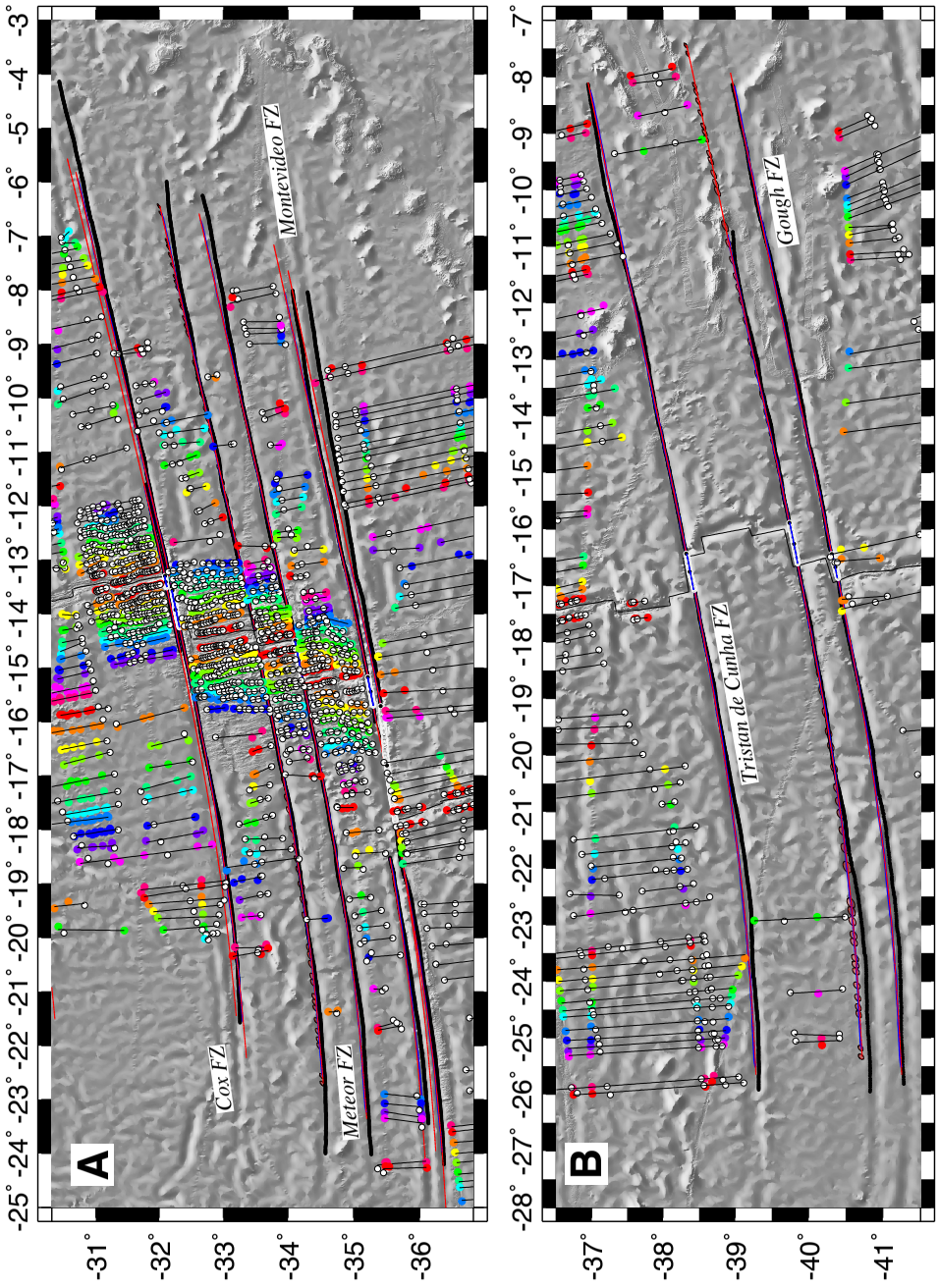


Supplemental Figure 7. Reconstructed (blue and red) and digitized (black) Nubia-South America fracture zone flow lines and transform faults and fracture zone crossings overlaid on GeoMapApp bathymetry, 30°S-42°S. See the caption to Supplemental Figure 4 for further information.

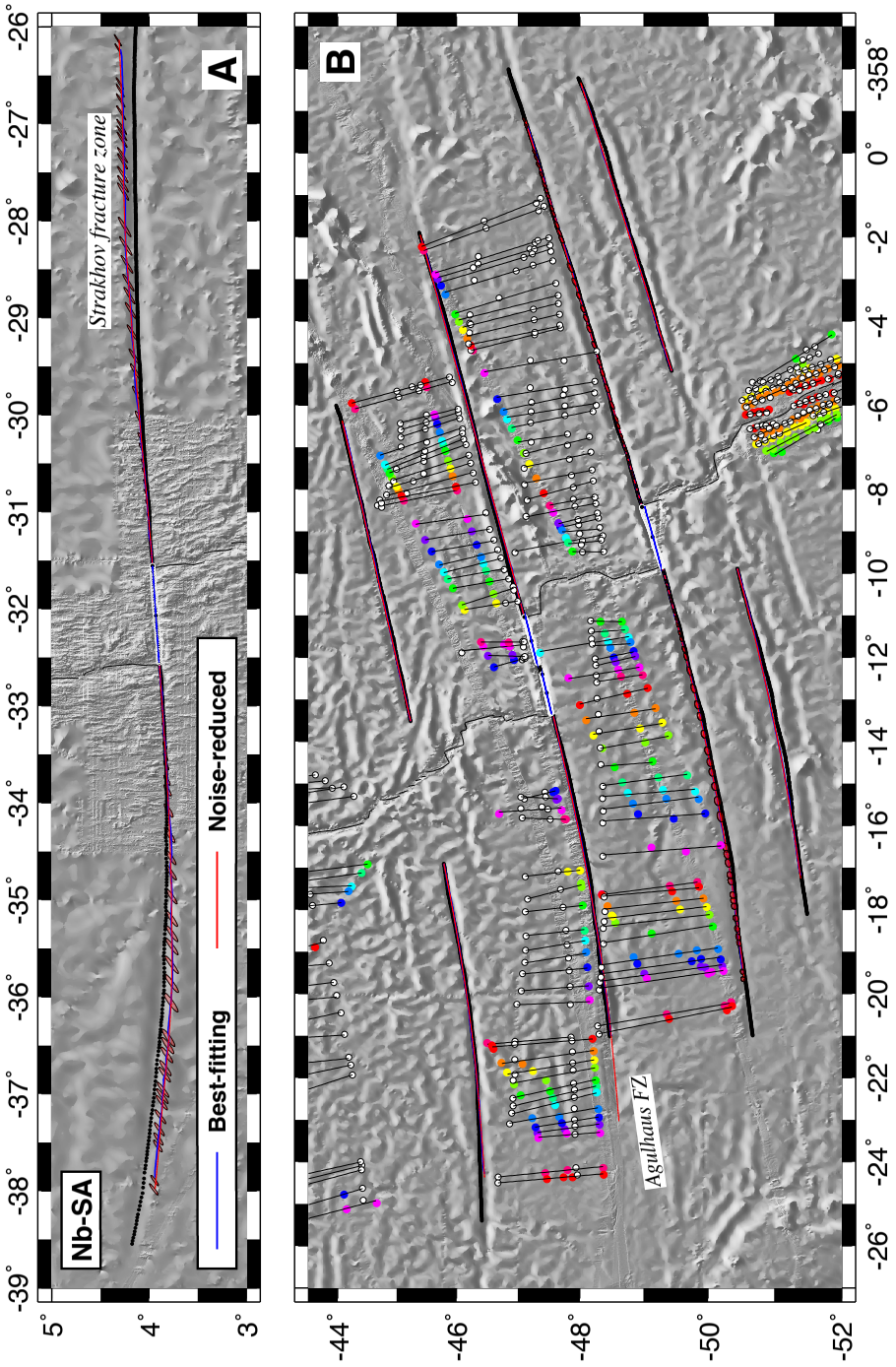


Supplemental Figure 8. Reconstructed (blue and red) and digitized (black) Nubia-South America fracture zone flow lines and transform faults and fracture zone crossings overlaid on GeoMapApp bathymetry. Panel A shows the Strakhov flow line north of the equator and Panel B shows 44°S-52°S fracture zones. See the caption to Supplemental Figure 4 for further information.